Modelling and simulation of fires in vehicle tunnels

I. Gasser, J. Struckmeier[*,†] and I. Teleaga

Department of Mathematics, University of Hamburg, Bundesstr. 55, Hamburg 20146, Germany

SUMMARY

Applying a low-Mach asymptotic for the compressible Navier–Stokes equations, we derive a new fluid dynamics model, which should be capable to model large temperature differences in combination with the low-Mach number limit. The model is used to simulate fires in vehicle tunnels, where the standard Boussinesq-approximation for the incompressible Navier–Stokes seems to be inappropriate due to the high temperatures developing in the tunnel. The model is implemented using a modified finite-difference approach for the incompressible Navier–Stokes equations and tested in some realistic fire events. Copyright © 2004 John Wiley & Sons, Ltd.

KEY WORDS: Navier–Stokes equations; non-Boussinesq approximation; low-Mach number limit

1. INTRODUCTION

Severe fire accidents in European vehicle tunnels during the past years have arised the question on how to improve the safety regulations and evacuation plans in existing or presently projected vehicle tunnels. To get a better knowledge on heat and smoke propagation and the corresponding emergency strategies it is necessary to perform real fire experiments in existing tunnels, which are complicated and costly tasks and even forbidden in some European countries. Besides real experiments the numerical modelling using computer simulations becomes more and more necessary and even tractable.

Up to now computer simulations in engineering sciences are nearly exclusively based on the so-called zonal models. In a zonal model the tunnel is divided into certain number of zones and each zone is characterized by some numerical quantities describing the (averaged) temperature, the mass fraction when considering chemical models as well as some other typical flow characteristics. Then each zone is coupled with its neighbours based on some heuristic balance equations, see References [1, 2].

A more fundamental approach is to use a field model, i.e. to use equations from computational fluid dynamics, like the well-known compressible Navier–Stokes equations, and to perform simulations based on these partial differential equations. In order to use a model

---

[*]Correspondence to: J. Struckmeier, Department of Mathematics, University of Hamburg, Bundesstr. 55, 20146 Hamburg, Germany.
[†]E-mail: struckmeier@math.uni-hamburg.de

from computational fluid dynamics one should decide whether the flow under consideration is compressible or incompressible, viscous or inviscid, laminar or turbulent and whether energy transport plays a significant role. First of all, the typical velocities in a vehicle tunnel are of the order of $1 \, \mathrm{m \, s}^{-1}$, which means that we are close to the low-Mach number limit, where the fluid becomes incompressible. On the other hand it is clear that during a fire event the energy transport is crucial to model the heat propagation correctly.

Incompressible viscous fluids are usually described by the incompressible Navier–Stokes equations, which are extended to energy transport using the so-called Boussinesq-approximation [3, 4]. Nevertheless, this model seems to be inappropriate to describe fire events, because the validity of the Boussinesq-approximation is restricted to small temperature differences. To describe large temperature variations one should use the compressible Navier–Stokes equations, but it is known that this model is inappropriate when considering the low-Mach number limit.

In the present paper we will study a new fluid dynamics model, which is capable to combine the low-Mach number limit with large temperature deviations occurring in the flow. The model is derived using a low-Mach number asymptotic for the compressible Navier–Stokes equations, where the fire in the tunnel is modelled by heat sources in the energy equation of the Navier–Stokes system.

2. THE NAVIER–STOKES SYSTEM WITH SOURCE TERMS

The starting point for the description of the flow propagation in the tunnel during a fire event are the compressible Navier–Stokes equations [5]. Additionally, the fire is modelled by a heat source in the energy equation, which represents a heat release rate inside a given volume, where the fire takes place. This method leads to a rather correct energy distribution inside the tunnel volume.

Hence, the two-dimensional compressible Navier–Stokes equations with source terms are written as

$$(\tilde{\rho})_{\tilde{t}} + \mathrm{div}(\tilde{\rho}\tilde{\mathbf{u}}) = 0$$

$$\tilde{\mathbf{u}}_{\tilde{t}} + (\tilde{\mathbf{u}} \cdot \nabla)\tilde{\mathbf{u}} + \frac{1}{\tilde{\rho}} \nabla \tilde{p} = \frac{\mu}{\tilde{\rho}} \Delta \tilde{\mathbf{u}} + \tilde{\mathbf{f}} \qquad (1)$$

$$(c_{\mathrm{v}}\tilde{\rho}\tilde{T})_{\tilde{t}} + \mathrm{div}(c_{\mathrm{v}}\tilde{\mathbf{u}}\tilde{\rho}\tilde{T}) + \tilde{p}\,\mathrm{div}(\tilde{\mathbf{u}}) = \lambda\Delta\tilde{T} + \tilde{q}$$

where $\tilde{\rho}(\mathbf{x}, t)$, $\tilde{\mathbf{u}}(\mathbf{x}, t) = (\tilde{u}, \tilde{v})^{\mathrm{T}}$, $\tilde{p}(\mathbf{x}, t)$, $\tilde{T}(\mathbf{x}, t)$ denote the density, the velocity, the pressure and the temperature of the fluid, respectively (see also Reference [6]).

The quantities μ, λ, c_p and c_{v} describe the dynamic viscosity, the heat conductivity and the specific heat coefficients under constant pressure and constant volume, respectively.

The term $\tilde{\mathbf{f}} = (\tilde{f}_x, \tilde{f}_y)^{\mathrm{T}}$ models the external forces, e.g. the gravitational force.

The source term $\tilde{q}$ consists of three contributions, i.e.

$$\tilde{q} = \tilde{q}_{\mathrm{w}} + \tilde{q}_{\mathrm{h}} + \tilde{q}_{\mathrm{s}}$$

where $\tilde{q}_{\mathrm{w}}$ is the heat conduction through the wall, $\tilde{q}_{\mathrm{h}}$ is the heat source and $\tilde{q}_{\mathrm{s}}$ is the sink source.

In many instances a compressible fluid can be regarded as a perfect gas, even if viscous effects are taken into account and the equation of state is written as

$$\tilde{p} = \tilde{\rho} R \tilde{T}$$

where $R = c_p - c_v$ is the gas constant.

System (1) is non-dimensionalized using the following scales:

$$x := \frac{\tilde{x}}{h}, \quad y := \frac{\tilde{y}}{h}, \quad t := \frac{u_\infty \tilde{t}}{h}$$

$$\mathbf{u} := \frac{\tilde{\mathbf{u}}}{u_\infty}, \quad p := \frac{\tilde{p}}{p_\infty}, \quad \rho := \frac{\tilde{\rho}}{\rho_\infty}, \quad T := \frac{\tilde{T}}{T_\infty}, \quad p_\infty = \rho_\infty R T_\infty \tag{2}$$

where h is the height of the tunnel. Typical values for the reference quantities in the case of long tunnels are (see also Reference [6])

$$u_\infty = 1 \text{ m s}^{-1}, \quad p_\infty = 10^5 \text{ kg m}^{-1} \text{ s}^{-1}, \quad \rho_\infty = 1.2 \text{ kg m}^{-3}, \quad T_\infty = 300 \text{ K}$$

Reformulating system (1) in the new variables (2) leads to

$$(\rho)_t + \text{div}(\rho \mathbf{u}) = 0$$

$$\mathbf{u}_t + (\mathbf{u} \cdot \nabla)\mathbf{u} + \frac{1}{\gamma M^2} \frac{1}{\rho} \nabla p = \left(\frac{1}{Re}\right) \frac{1}{\rho} \Delta \mathbf{u} + \mathbf{f} \tag{3}$$

$$(\rho T)_t + \text{div}(\mathbf{u} \rho T) + (\gamma - 1) p \, \text{div}(\mathbf{u}) = \left(\frac{\gamma}{Pr} \frac{1}{Re}\right) \Delta T + q$$

where the adiabatic exponent γ, the Mach number M, the Reynold's number Re, the Prandl number Pr and the Froude number Fr are given by

$$\gamma = \frac{c_p}{c_v}, \quad M^2 = \frac{\rho_\infty u_\infty^2}{\gamma p_\infty}, \quad Re = \frac{\rho_\infty u_\infty h}{\mu}, \quad Pr = \frac{\mu c_p}{\lambda}, \quad Fr := \frac{u_\infty}{\sqrt{h \|\vec{\mathbf{f}}\|}}$$

$$\text{with } \mathbf{f} = \frac{\tilde{\mathbf{f}}}{Fr^2 \|\tilde{\mathbf{f}}\|}, \quad q = \frac{q_\infty h}{u_\infty p_\infty} (\gamma - 1) \tilde{q}$$

The values corresponding to these parameters can be found in Reference [6]. It turns out that the Mach number M is of the order of 10^{-5} and therefore we use an asymptotic expansion for the pressure in the low-Mach number regime given by

$$p = p_0 + \varepsilon p_1 + O(\varepsilon^2) \tag{4}$$

where $\varepsilon = \gamma M^2$. Inserting formula (4) into system (3), the momentum equation yields in leading order

$$\nabla p_0 = 0 \quad \Rightarrow \quad p_0 = p_0(t)$$

But, assuming that the ground pressure in a open domain is also constant in time, we can conclude that p_0 is constant in time. Using the leading order approximation $T = p_0/\rho$ from

the third equation of system (3), we obtain

$$\mathrm{div}(\mathbf{u}) = \frac{q}{\gamma p_0} \tag{5}$$

Finally, system (3) is transformed into

$$(\rho)_t + \mathrm{div}(\rho \mathbf{u}) = 0 \tag{6}$$

$$\mathbf{u}_t + (\mathbf{u} \cdot \nabla)\mathbf{u} + \frac{1}{\rho} \nabla p_1 = \left(\frac{1}{Re}\right) \frac{1}{\rho} \Delta \mathbf{u} + \mathbf{f} \tag{7}$$

$$\mathrm{div}(\mathbf{u}) = Q \tag{8}$$

where Q is the right-hand side of Equation (5). One should notice that this are not the incompressible Navier–Stokes equations with variable density [7, 8, 3] because the velocity is not divergence-free.

System (6)–(8) is considered as an initial–boundary value problem on a bounded, rectangular domain Ω with boundary $\partial\Omega$ given by

$$\partial\Omega = \Gamma_1 \cap \Gamma_2 \cap \Gamma_3 \cap \Gamma_4$$

Here, Γ_1 and Γ_3 denote the entrance and exit of the tunnel, Γ_2 and Γ_4 the lower and upper fixed wall, respectively.

The initial conditions are given by

$$\rho(\mathbf{x}, 0) = \rho_0(\mathbf{x}), \quad \mathbf{u}(\mathbf{x}, 0) = \mathbf{u}_0(\mathbf{x}), \quad p_1(x, 0) = p_{10}(x) \quad (\forall x \in \Omega) \tag{9}$$

The boundary conditions for the velocity are

$$\frac{\partial \mathbf{u}}{\partial x}(\mathbf{x}, t) = 0, \quad \mathbf{x} \in \Gamma_1 \cup \Gamma_3$$
$$\mathbf{u}(\mathbf{x}, t) = 0, \quad \mathbf{x} \in \Gamma_2 \cup \Gamma_4 \tag{10}$$

For the density, we use standard inflow conditions

$$\rho(\mathbf{x}, t) = \rho_0 \quad \text{if } \mathbf{u}(\mathbf{x}, t) > 0, \ \mathbf{x} \in \Gamma_1$$
$$\rho(\mathbf{x}, t) = \rho_1 \quad \text{if } \mathbf{u}(\mathbf{x}, t) < 0, \ \mathbf{x} \in \Gamma_3 \tag{11}$$

A very sensitive task is to impose boundary conditions for the pressure. In order to do this we transform our system (6)–(8) applying the divergence operator to Equation (7) (assuming enough differentiability), which yields a non-linear Poisson equation for the pressure

$$\mathrm{div}\left(\frac{1}{\rho} \nabla p_1\right) = \mathrm{div}\left(\frac{1}{Re} \frac{1}{\rho} \Delta \mathbf{u} + \mathbf{f}\right) - Q\mathbf{u} \cdot \nabla \mathbf{u} - \nabla(\mathbf{u} \cdot \nabla \mathbf{u}) \cdot \mathbf{u} - Q_t \tag{12}$$

The boundary conditions are

$$p_1(\mathbf{x}, t) = p(\mathbf{x}) \quad \text{on } \Gamma_1 \cup \Gamma_3 \tag{13}$$

$$\nabla p_1 \cdot \vec{n} = \left(\frac{1}{Re} \frac{1}{\rho} \Delta \mathbf{u} + \mathbf{f} \right) \cdot \vec{n} \quad \text{on } \Gamma_2 \cup \Gamma_4 \tag{14}$$

where $\vec{n}$ is the exterior unit normal vector.

Remark

(i) Using Dirichlet boundary conditions for pressure at the entrance and exit of the tunnel, we can directly simulate atmospheric effects or a pressure profile induced by ventilators. It is known that a ventilator produces an overpressure which induces a certain velocity to the fluid.
(ii) The Neumann boundary conditions for the pressure at the top and the bottom of the domain are derived by taking the normal component of Equation (7) at the boundary and using the prescribed boundary conditions for the velocity field.

   In the next section, we will solve numerically the following system obtained from Equations (6)–(8):

$$(\rho)_t + \text{div}(\rho \mathbf{u}) = 0 \tag{15}$$

$$\mathbf{u}_t + (\mathbf{u} \cdot \nabla)\mathbf{u} + \frac{1}{\rho} \nabla p_1 = \left(\frac{1}{Re} \right) \frac{1}{\rho} \Delta \mathbf{u} + \mathbf{f} \tag{16}$$

$$\text{div} \left(\frac{1}{\rho} \nabla p_1 \right) = \text{div} \left(\frac{1}{Re} \frac{1}{\rho} \Delta \mathbf{u} + \mathbf{f} \right) - Q\mathbf{u} \cdot \nabla \mathbf{u} - \nabla(\mathbf{u} \cdot \nabla \mathbf{u}) \cdot \mathbf{u} - Q_t \tag{17}$$

together with the initial conditions (9) and the boundary conditions (10), (11), (13) and (14).

3. THE NUMERICAL SCHEME

The numerical solution of system (15)–(17) is realized using an algorithm based on the *Marker and Cell* (*MAC*) method [9]. This method consists of a simple finite difference scheme with an explicit first-order time discretization. The domain is discretized using a *staggered* grid, in which the unknowns are not located at the same grid points. The discrete values for the velocities, the pressure and the density are located on three separate grids, each shifted by half a grid spacing to the bottom, to the left, and to the lower left, respectively (see Figure 1).

   The finite difference notations used here are: p_{ij}^n is the pressure at the centre of cell (i, j) at time level n; ρ_{ij}^n the density at the centre of cell (i, j) at time level n; u_{ij}^n the velocity in x direction at the middle of right side of cell (i, j) at time level n and v_{ij}^n the velocity in y direction at the middle of top side of cell (i, j) at time level n.

   Subscripts are used for the cell location and superscripts for the time level at which the quantities are evaluated such that $t = n\Delta t$, where Δt is the time step.
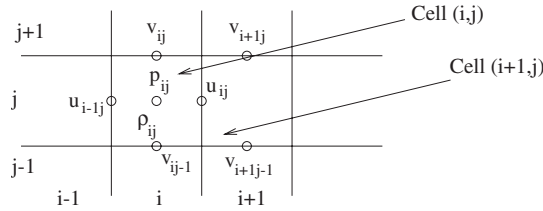
Figure 1. The staggered grid.
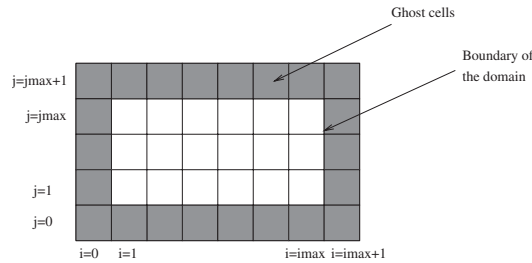
Figure 2. The cell displacement.

Using this grid we can see that not all the values are lying at the boundary of the domain, e.g. the values of v. Therefore, the domain is surrounded by a single layer of the so-called *ghost* cells, see Figure 2.

3.1. Time discretization

The time derivatives appearing in system (15)–(17) are discretized using a first-order forward Euler method. First, the density ρ^{n+1} is found from Equation (15). Then, to find $\mathbf{u}^{n+1}$ and p^{n+1} from (16) and (17) we use an *adapted* projection method.

This means that in the first step an auxiliary velocity field $\mathbf{u}^{\text{aux}}$ is computed from the following equation:

$$\frac{\mathbf{u}^{\text{aux}} - \mathbf{u}^n}{\Delta t} + [(\mathbf{u} \cdot \nabla)\mathbf{u}]^n = \frac{1}{Re} \frac{[\Delta \mathbf{u}]^n}{\rho^{n+1}} + \mathbf{f}^n$$

$$\frac{\partial \mathbf{u}^{\text{aux}}}{\partial n} = w \quad \text{on } \partial\Omega \tag{18}$$

The quantity w is computed such that $\text{div}(\mathbf{u}) = Q$ on $\partial\Omega$ (see Section 3.3).

In the second step, the velocity $\mathbf{u}^{n+1}$ is found from:

$$\mathbf{u}^{n+1} = \mathbf{u}^{\text{aux}} - \frac{\Delta t}{\rho^{n+1}} \nabla p^{n+1} \tag{19}$$

$$\nabla \mathbf{u}^{n+1} = Q \tag{20}$$

In order to find p^{n+1} we derive the discrete version of Equation (17). This can be obtained by taking the divergence of Equation (19) and using Equation (20).

Now, we will write in more details the method explained above. First we rewrite the convective terms in Equation (16) using the continuity Equation (8)

$$u^{n+1} = u^n + \Delta t \left(\frac{1}{Re} \frac{1}{\rho^{n+1}} \left[\left(\frac{\partial^2 u}{\partial x^2} + \frac{\partial^2 u}{\partial y^2} \right) \right]^n - \left[\frac{\partial (u^2)}{\partial x} \right]^n - \left[\frac{\partial (uv)}{\partial y} \right]^n \right.$$

$$\left. + [uQ + f_x]^n - \left[\frac{1}{\rho} \frac{\partial p}{\partial x} \right]^{n+1} \right) \qquad (21)$$

$$v^{n+1} = v^n + \Delta t \left(\frac{1}{Re} \frac{1}{\rho^{n+1}} \left[\left(\frac{\partial^2 v}{\partial x^2} + \frac{\partial^2 v}{\partial y^2} \right) \right]^n - \left[\frac{\partial (uv)}{\partial x} \right]^n - \left[\frac{\partial (v^2)}{\partial y} \right]^n \right.$$

$$\left. + [vQ + f_y]^n - \left[\frac{1}{\rho} \frac{\partial p}{\partial y} \right]^{n+1} \right) \qquad (22)$$

Using Equation (18) we can write

$$u^{\mathrm{aux}} := u^n + \Delta t \left(\frac{1}{Re} \frac{1}{\rho^{n+1}} \left[\left(\frac{\partial^2 u}{\partial x^2} + \frac{\partial^2 u}{\partial y^2} \right) \right]^n - \left[\frac{\partial (u^2)}{\partial x} \right]^n - \left[\frac{\partial (uv)}{\partial y} \right]^n \right.$$

$$\left. + [uQ + f_x]^n \right)$$

$$v^{\mathrm{aux}} := v^n + \Delta t \left(\frac{1}{Re} \frac{1}{\rho^{n+1}} \left[\left(\frac{\partial^2 v}{\partial x^2} + \frac{\partial^2 v}{\partial y^2} \right) \right]^n - \left[\frac{\partial (uv)}{\partial x} \right]^n - \left[\frac{\partial (v^2)}{\partial y} \right]^n \right.$$

$$\left. + [vQ + f_y]^n \right)$$

to obtain

$$u^{n+1} = u^{\mathrm{aux}} - \Delta t \frac{1}{\rho^{n+1}} \frac{\partial p^{n+1}}{\partial x} \qquad (23)$$

$$v^{n+1} = v^{\mathrm{aux}} - \Delta t \frac{1}{\rho^{n+1}} \frac{\partial p^{n+1}}{\partial y} \qquad (24)$$

Using again Equation (20), we get from Equations (23) and (24)

$$Q = \frac{\partial u^{n+1}}{\partial x} + \frac{\partial v^{n+1}}{\partial y} = \frac{\partial u^{\mathrm{aux}}}{\partial x} + \frac{\partial v^{\mathrm{aux}}}{\partial y} - \Delta t \left[\frac{1}{\rho^{n+1}} \left(\frac{\partial^2 p^{n+1}}{\partial x^2} + \frac{\partial^2 p^{n+1}}{\partial y^2} \right) \right.$$

$$\left. - \frac{1}{(\rho^{n+1})^2} \left(\frac{\partial \rho^{n+1}}{\partial x} \frac{\partial p^{n+1}}{\partial x} + \frac{\partial \rho^{n+1}}{\partial y} \frac{\partial p^{n+1}}{\partial y} \right) \right]$$

which, after rearranging, becomes a *non-linear* Poisson equation for the pressure p^{n+1} at time t_{n+1}

$$\frac{\partial^2 p^{n+1}}{\partial x^2} + \frac{\partial^2 p^{n+1}}{\partial y^2} - \frac{1}{\rho^{n+1}} \left(\frac{\partial \rho^{n+1}}{\partial x} \frac{\partial p^{n+1}}{\partial x} + \frac{\partial \rho^{n+1}}{\partial y} \frac{\partial p^{n+1}}{\partial y} \right)$$

$$= \frac{\rho^{n+1}}{\Delta t} \left[\frac{\partial u^{\mathrm{aux}}}{\partial x} + \frac{\partial v^{\mathrm{aux}}}{\partial y} \right] - \frac{Q \rho^{n+1}}{\Delta t} \tag{25}$$

Finally, $\mathbf{u}^{n+1}$ is updated using Equation (19).

3.2. Spatial discretization

Now, we have to discretize all spatial derivatives appearing in the semi-discrete equations derived in the previous section. For the spatial discretization of the density Equation (15) we use a standard upwind method

$$\rho_{ij}^{n+1} = \rho_{ij}^n - u_{ij}^+ \frac{\Delta t}{\Delta x}(\rho_{ij}^n - \rho_{i-1j}^n) - u_{ij}^- \frac{\Delta t}{\Delta x}(\rho_{i+1j}^n - \rho_{ij}^n)$$

$$- v_{ij}^+ \frac{\Delta t}{\Delta y}(\rho_{ij}^n - \rho_{ij-1}^n) - v_{ij}^- \frac{\Delta t}{\Delta y}(\rho_{ij+1}^n - \rho_{ij}^n) - \Delta t \rho_{ij}^n Q_{ij}^n \tag{26}$$

where

$$\mathbf{u}^+ = \max(\mathbf{u}, 0) = \tfrac{1}{2}(\mathbf{u} + |\mathbf{u}|), \quad \mathbf{u}^- = \min(\mathbf{u}, 0) = \tfrac{1}{2}(\mathbf{u} - |\mathbf{u}|).$$

The spatial discretization of Equations (23) and (24) is

$$u_{ij}^{n+1} = u_{ij}^{\mathrm{aux}} - \frac{\Delta t}{\Delta x} \frac{1}{\rho_{ij}^{n+1}} (p_{i+1j}^{n+1} - p_{ij}^{n+1})$$

$$i = 1, \ldots, i_{\max} - 1, \quad j = 1, \ldots, j_{\max} \tag{27}$$

$$v_{ij}^{n+1} = v_{ij}^{\mathrm{aux}} - \frac{\Delta t}{\Delta y} \frac{1}{\rho_{ij}^{n+1}} (p_{ij+1}^{n+1} - p_{ij}^{n+1})$$

$$i = 1, \ldots, i_{\max}, \quad j = 1, \ldots, j_{\max} - 1 \tag{28}$$

The Laplace operator appearing in the equations of u^{aux} are discretized using the standard 5-point stencil. Some difficulties appear when we discretize the convective terms $\partial(u^2)/\partial x$, $\partial(uv)/\partial y$, $\partial(uv)/\partial x$, and $\partial(v^2)/\partial y$. Because the convective terms become dominant at high Reynold's numbers, it is necessary to use a mixture of the central differences and the donor-cell discretization (see References [10, 11]).

As an example, we give here the discretization of the convective term $\partial(u^2)/\partial x$ evaluated at the mid-point of the right edge of cell (i,j), $i=1,\ldots,i_{\max}-1$, $j=1,\ldots,j_{\max}$

$$\left[\frac{\partial(u^2)}{\partial x}\right]_{i,j} := \frac{1}{\Delta x}\left(\left(\frac{u_{i,j}+u_{i+1,j}}{2}\right)^2 - \left(\frac{u_{i-1,j}+u_{i,j}}{2}\right)^2\right)$$

$$+\gamma\frac{1}{\Delta x}\left(\frac{|u_{i,j}+u_{i+1,j}|(u_{i,j}-u_{i+1,j})}{4} - \frac{|u_{i-1,j}+u_{i,j}|(u_{i-1,j}-u_{i,j})}{4}\right)$$

where the parameter γ is chosen between $[0,1]$, $\gamma=0$ corresponds to central differences, while $\gamma=1$ yields the donor-cell scheme.

The discrete Poisson equation for pressure is

$$\frac{p_{i+1j}^{n+1} - 2p_{ij}^{n+1} + p_{i-1j}^{n+1}}{(\Delta x)^2} + \frac{p_{ij+1}^{n+1} - 2p_{ij}^{n+1} + p_{ij-1}^{n+1}}{(\Delta y)^2}$$

$$-\frac{1}{\rho_{ij}^{n+1}}\left[\frac{\rho_{i+1j}^{n+1} - \rho_{i-1j}^{n+1}}{2\Delta x}\frac{p_{i+1j}^{n+1} - p_{i-1j}^{n+1}}{2\Delta x} + \frac{\rho_{ij+1}^{n+1} - \rho_{ij-1}^{n+1}}{2\Delta y}\frac{p_{ij+1}^{n+1} - p_{ij-1}^{n+1}}{2\Delta y}\right]$$

$$=\frac{\rho_{ij}^{n+1}}{\Delta t}\left[\frac{u_{ij}^{\mathrm{aux}} - u_{i-1j}^{\mathrm{aux}}}{\Delta x} + \frac{v_{ij}^{\mathrm{aux}} - v_{ij-1}^{\mathrm{aux}}}{\Delta y}\right] - \frac{Q_{ij}\rho_{ij}^{n+1}}{\Delta t}$$

$$i=1,\ldots,i_{\max}, \quad j=1,\ldots,j_{\max} \tag{29}$$

3.3. Boundary conditions

The discrete boundary conditions for the velocities read as

$$\left.\begin{array}{ll} u_{0,j}=u_{1,j}, & u_{i_{\max},j}=u_{i_{\max}-1,j} \\ v_{0,j}=v_{1,j}, & v_{i_{\max}+1,j}=v_{i_{\max},j} \end{array}\right\} \quad \text{for } j=1,\ldots,j_{\max}$$

$$\left.\begin{array}{ll} u_{i,0}=-u_{i,1}, & u_{i,j_{\max}+1}=-u_{i,j_{\max}} \\ v_{i,0}=0, & v_{i,j_{\max}}=0 \end{array}\right\} \quad \text{for } i=1,\ldots,i_{\max}$$

Additionally, we need the following values of u^{aux}, v^{aux} at the boundary in order to compute the right-hand side of Equation (29)

$$u_{0,j}^{\mathrm{aux}}, \ u_{i_{\max},j}^{\mathrm{aux}} \quad \text{for } j=1,\ldots,j_{\max}$$

$$v_{i,0}^{\mathrm{aux}}, \ v_{i,j_{\max}}^{\mathrm{aux}} \quad \text{for } i=1,\ldots,i_{\max}$$

which have been not yet specified.

To determine these boundary values we take a look at Equations (27) and (28) evaluated at the boundaries. It turns out that we need the values of $u_{-1,j}$, $u_{i_{\max}+1,j}$, $v_{i,-1}$, $v_{i,j_{\max}+1}$ and to compute these values we use the discrete boundary conditions and the discretized continuity Equation (8) in the cells $(0,j)$, $(i_{\max},i)$, $(i,0)$, $(i,j_{\max})$.

Imposing the Dirichlet and Neumann boundary conditions for the pressure we get

$$p_{0,j} = 2p^{\text{in}} - p_{1,j},$$

$$p_{\text{imax}+1,j} = 2p^{\text{out}} - p_{\text{imax},j}, \quad j = 1,\ldots,j_{\max}$$

$$p_{i,0} = p_{i,1} - \frac{\Delta y}{\Delta t} \rho_{i,0} v_{i,0}^{\text{aux}},$$

$$p_{i,j_{\max}+1} = p_{i,j_{\max}} + \frac{\Delta y}{\Delta t} \rho_{i,j_{\max}} v_{i,j_{\max}}^{\text{aux}}, \quad i = 1,\ldots,i_{\max}$$

where p^{in}, p^{out} represent the hydrostatic pressures with respect to the height of the domain.

3.4. Stability condition

In order to ensure stability of the numerical scheme we have to impose stability conditions on the time step Δt. Usually, these conditions are of the form

$$\frac{2\Delta t}{Re} < \left(\frac{1}{(\Delta x)^2} + \frac{1}{(\Delta y)^2} \right)^{-1}, \quad |u_{\max}|\Delta t < \Delta x, \quad |v_{\max}|\Delta t < \Delta y \tag{30}$$

where $|u_{\max}|$, $|v_{\max}|$ are the maximal absolute values of the velocities. Based on these stability conditions an adaptive time step is computed in Reference [11], such that Δt for the next time step satisfies all conditions (30):

$$\Delta t < \tau \min \left(\frac{Re}{2} \left(\frac{1}{(\Delta x)^2} + \frac{1}{(\Delta y)^2} \right)^{-1}, \frac{\Delta x}{|u_{\max}|}, \frac{\Delta y}{|v_{\max}|} \right) \tag{31}$$

The factor $\tau \in]0,1]$ is a so-called safety factor. To solve the Poisson equation for pressure (29) we apply a standard BiCGSTAB-method.

4. NUMERICAL EXAMPLES

In the following we give numerical results for two realistic fire events in a vehicle tunnel. In both cases the heat source has a strength of 1 MW. The heat source is placed exactly in the middle of the tunnel and it is distributed over a rectangular area of size $10\,\text{m} \times 4\,\text{m}$. One should notice that the heat source is implemented as an indicator function and not as an obstacle. In the first example the tunnel profile has no slope, in the second one we consider a constant slope of 3%.

Table I. Data for a tunnel without slope.

Length	1 km
Height	10 m
Slope	0%
Heat source	1 MW
Pressure difference (bottom–top)	120 Pa
Simulation time	30 min
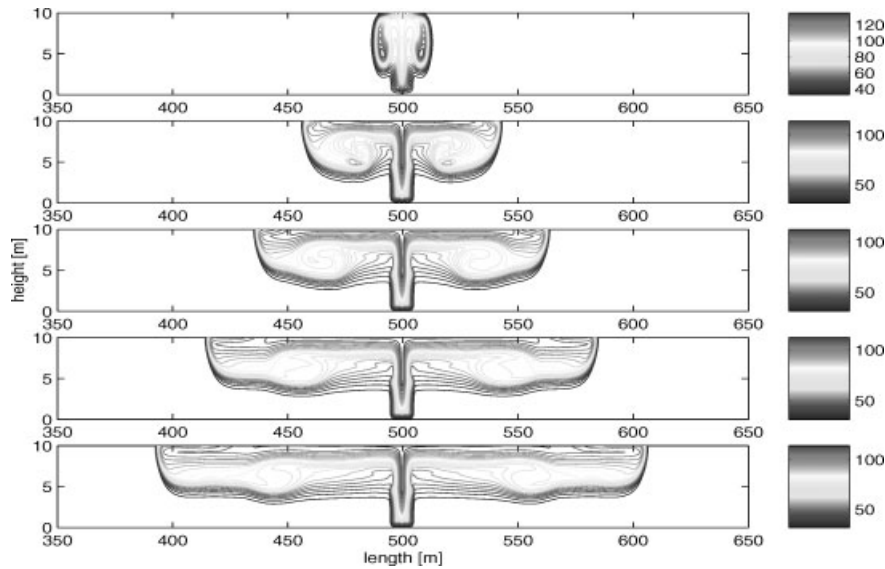
Figure 3. Development of the temperature field (in °C) for a tunnel without slope up to time $t = 1$ min. The horizontal axis represents the tunnel section between 350 and 650 m.

4.1. Tunnel without slope

The tunnel configuration and other relevant data are listed in Table I. As initial conditions we use

$$u_0(x) = v_0(x) = 0, \quad \rho_0(x) = 1.2, \quad P(y) = \rho \mathbf{g} y$$

where the value for the pressure is just the hydrostatic pressure. Figure 3 shows from top to bottom the time propagation of the temperature field at the discrete times $t = 10, 25, 35, 45$ s and 60 s for the tunnel section between 350 and 650 m. The corresponding results for the mean velocity are given in Figure 4. Because there is no pressure difference between the entrance and the exit of the tunnel (see also Figure 5) the fronts of the temperature (as well as the velocity) propagate symmetrically with respect to the middle of the tunnel.

Continuing the simulation from $t = 1$ min, we observe that the temperature and velocity front remain symmetric up to the end of the simulation at $t = 30$ min. Figures 6–8 show the temperature, the mean velocity and the pressure fields, respectively, at $t = 90, 105, 155$ s and
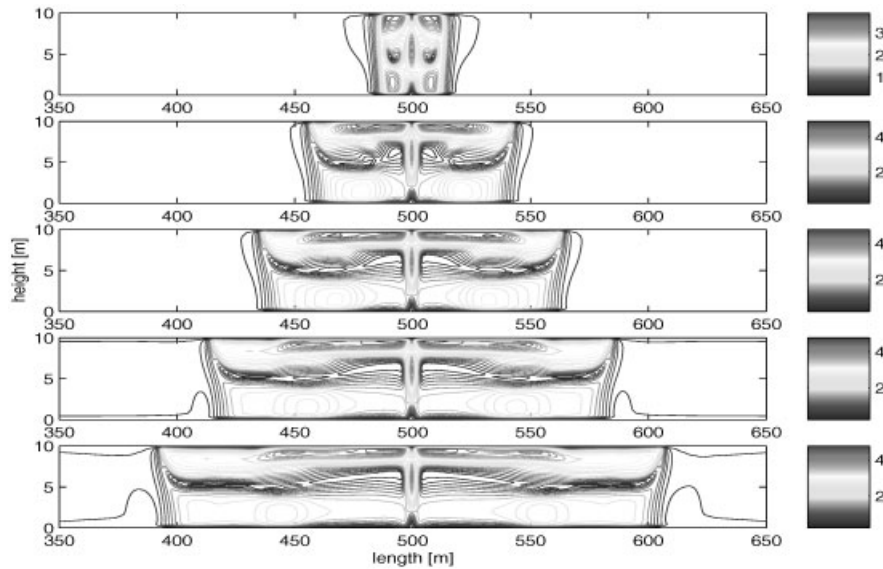
Figure 4. Development of the mean velocity field (in m s^{-1}) for a tunnel without slope up to time $t = 1$ min. The horizontal axis represents the tunnel section between 350 and 650 m.
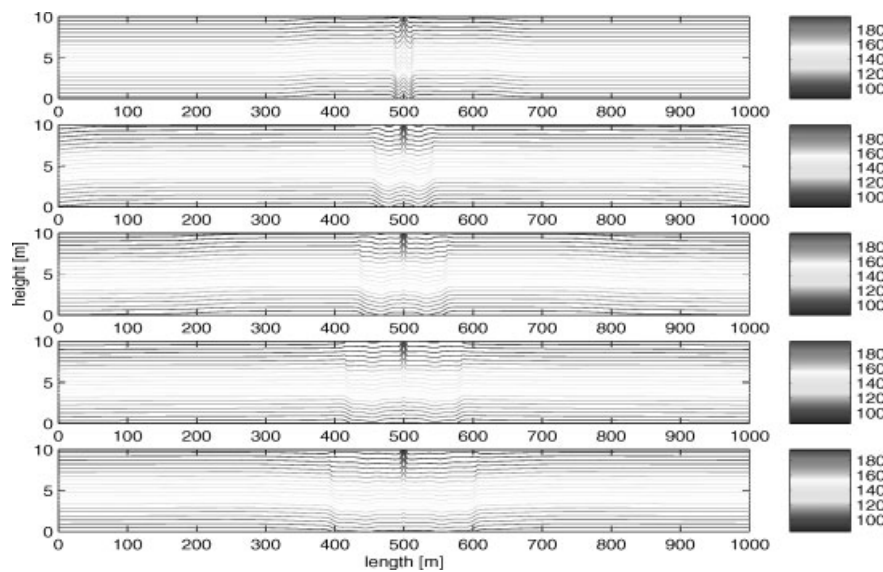
Figure 5. Development of the pressure field (in Pa) for a tunnel without slope up to time $t = 1$ min. The horizontal axis represents the whole tunnel length of 1000 m.
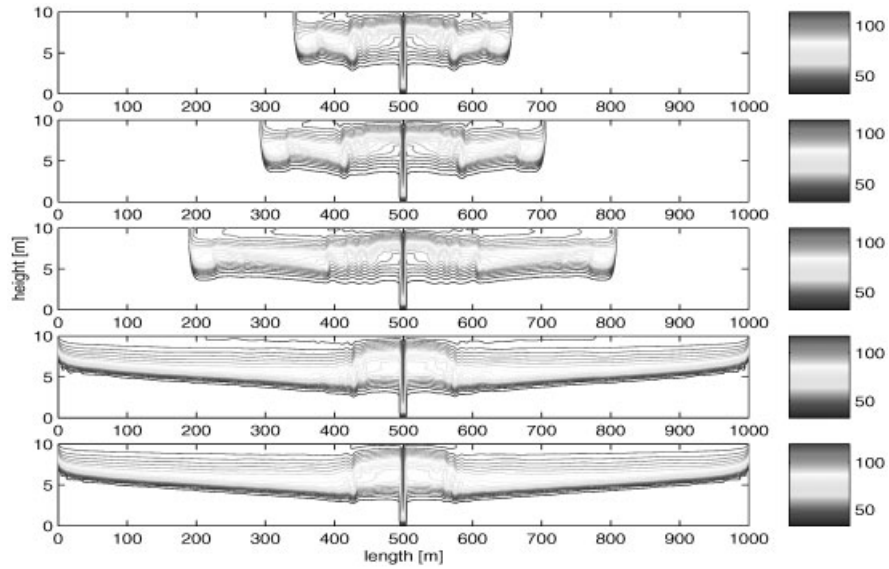
Figure 6. Development of the temperature field (in °C) for a tunnel without slope between $t = 1$ and 30 min. The horizontal axis represents the whole tunnel length of 1000 m.
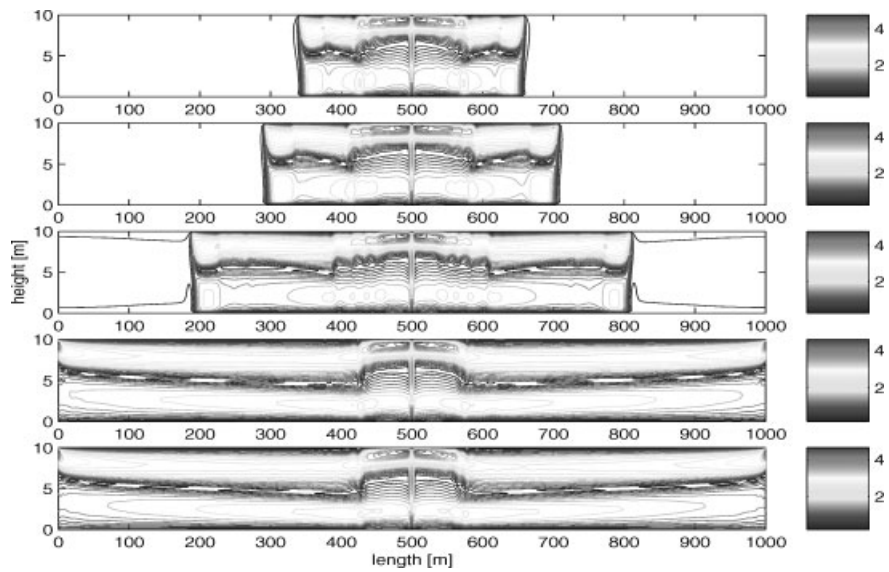
Figure 7. Development of the mean velocity field (in m s^{-1}) for a tunnel without slope between $t = 1$ and 30 min. The horizontal axis represents the whole tunnel length of 1000 m.
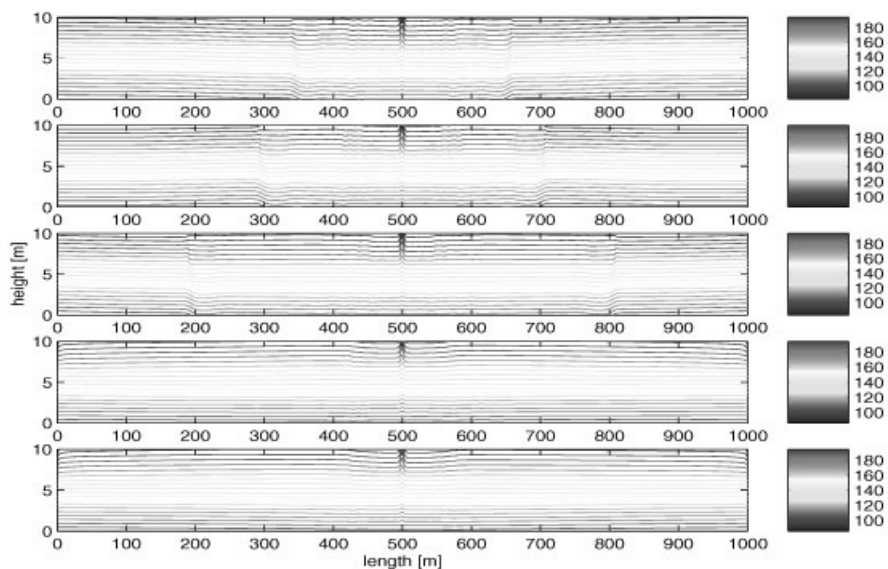
Figure 8. Development of the pressure field (in Pa) for a tunnel without slope between $t = 1$ and 30 min. The horizontal axis represents the whole tunnel length of 1000 m.

Table II. Data for a tunnel with slope.

Length	1 km
Height	10 m
Slope	3%
Heat source	1 MW
Pressure difference (bottom–top)	120 Pa
Simulation time	30 min

$t = 17, 30$ min, again from top to bottom. The horizontal axis in the figures now represents the whole tunnel length of 1km. The pressure nicely stabilizes to the given values. The results even show that there are no boundary instabilities caused by improper boundary conditions, which proves that the boundary conditions used are suitable conditions for our model equations.

4.2. Tunnel with slope

The tunnel configuration and other relevant data are listed in Table II. Now the tunnel profile has a slope of 3% and we use the same initial conditions like in the previous example. Figures 9–14 correspond to the description of the first example given by Figures 3–8.

As in the previous example, the largest speed of propagation of the fronts occurs at the beginning of the simulations in the neighbourhood of the heat source, see Figure 10. Here, because the tunnel profile has a slope of 3%, we do not observe a symmetric propagation of the fronts. Due to the pressure difference the front moves more fast to the right than to the left, see Figures 9, 10, 12 and 13. Due to the Reynold's number of $Re = 2500$ some vortex structures appear in the temperature and velocity field.
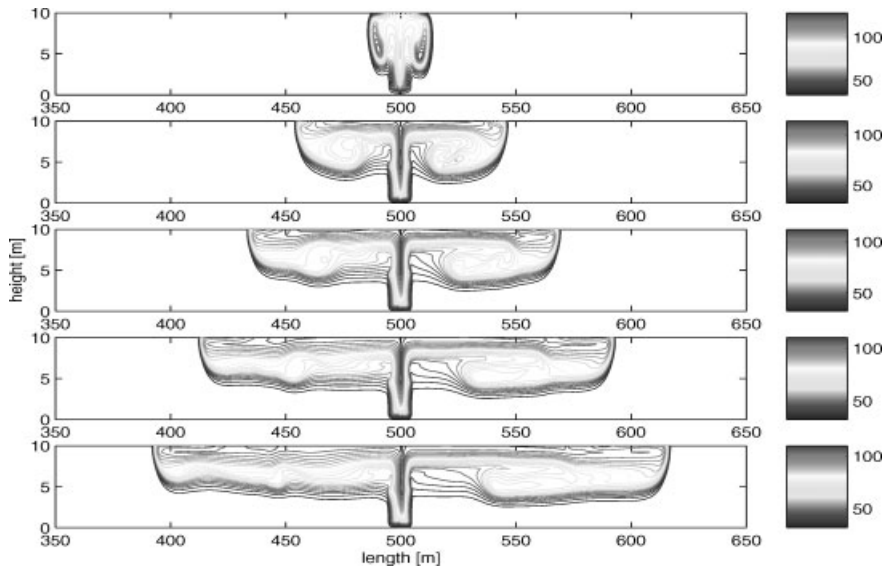
Figure 9. Development of the temperature field (in °C) for a tunnel with slope up to time $t = 1$ min. The horizontal axis belongs to the tunnel section between 350 and 650 m.
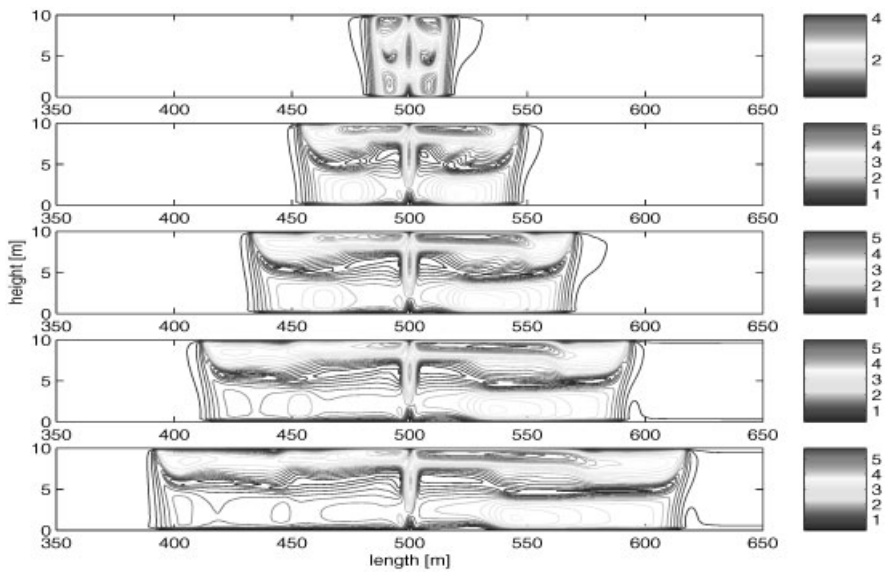
Figure 10. Development of the mean velocity field (in m s^{-1}) for a tunnel with slope up to time $t = 1$ min. The horizontal axis belongs to the tunnel section between 350 and 650 m.
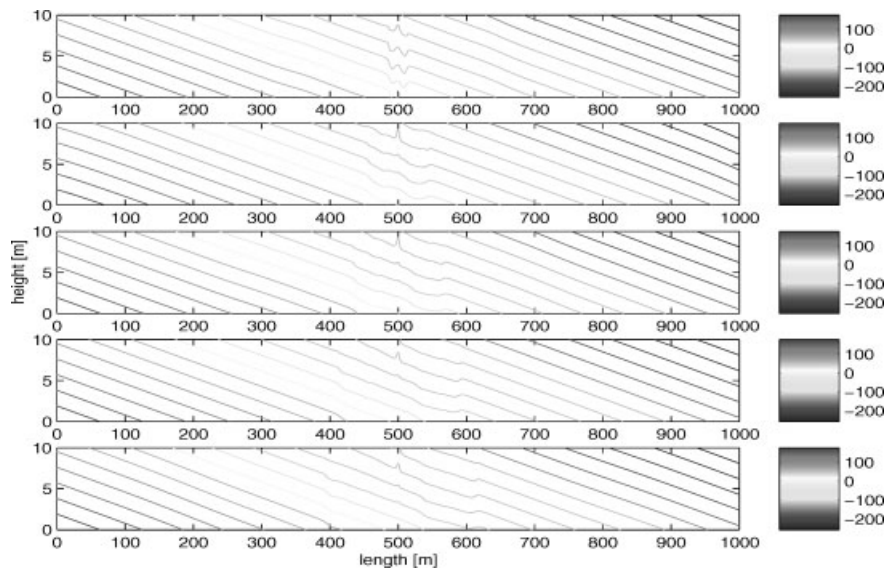
Figure 11. Development of the pressure field (in Pa) for a tunnel with slope up to time $t = 1$ min. The horizontal axis belongs the whole tunnel length of 1000 m.
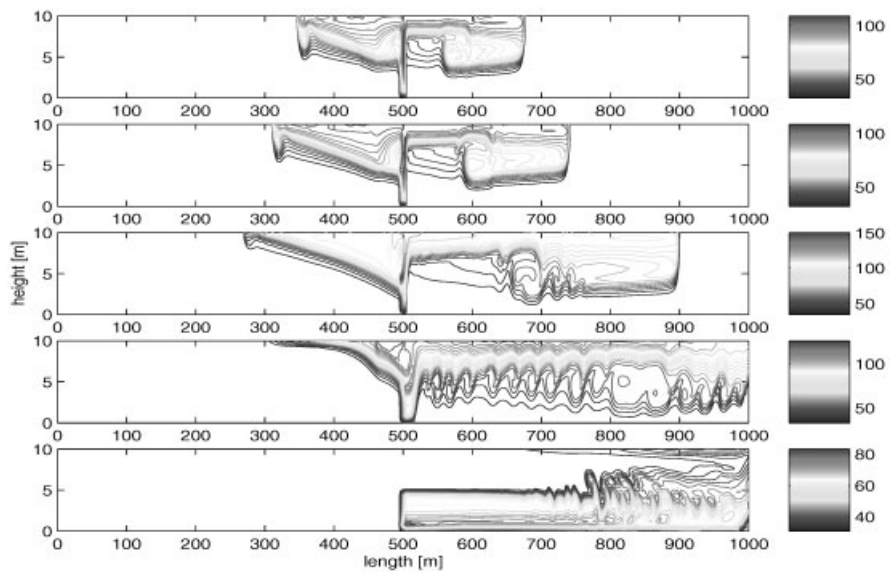
Figure 12. Development of the temperature field (in °C) for a tunnel with slope between $t = 1$ and 30 min. The horizontal axis represents the whole tunnel length of 1000 m.
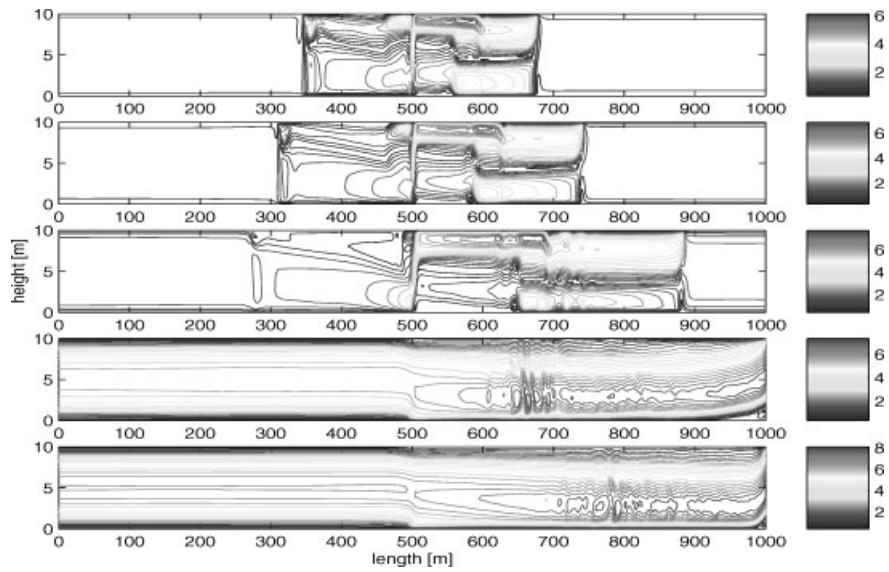
Figure 13. Development of the mean velocity field (in ms^{-1}) for a tunnel with slope between $t = 1$ and 30 min. The horizontal axis represents the whole tunnel length of 1000 m.
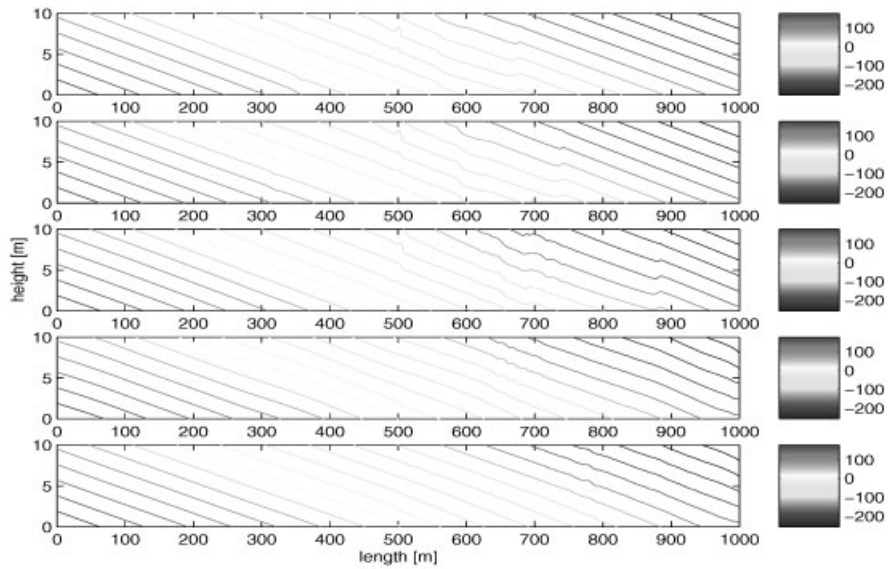
Figure 14. Development of the pressure field (in Pa) for a tunnel with slope between $t = 1$ and 30 min. The horizontal axis represents the whole tunnel length of 1000 m.

Int. J. Numer. Meth. Fluids 2004; **44**:277–296
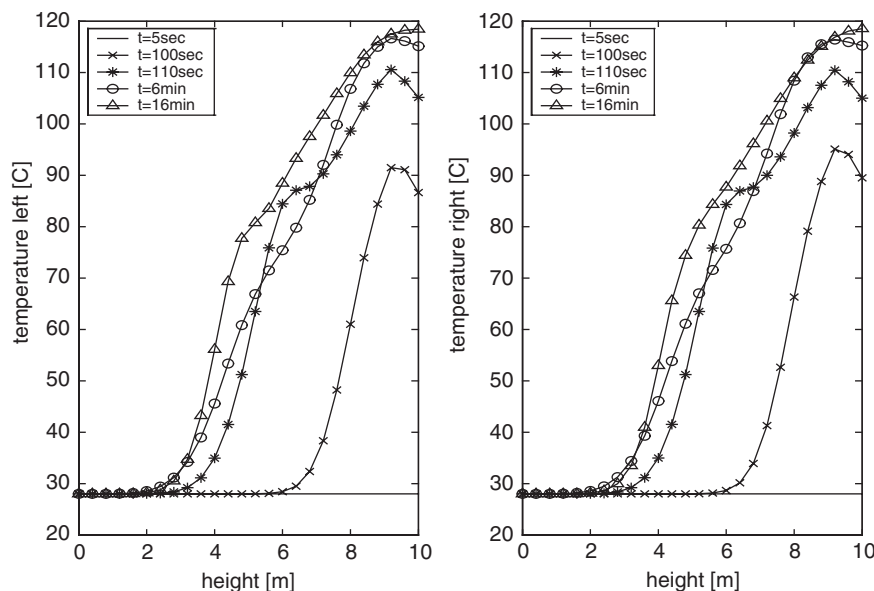
Figure 15. Vertical temperature profiles (in °C) for a tunnel without slope 100 m left and right from the heat source at various times.

Finally, Figures 15 and 16 show instantaneous temperature profiles at various times along a vertical axis, which is placed 100 m to the left and right of the middle of the tunnel for example I and II, respectively. Figure 15 shows, that even the vertical temperature profiles remain nearly symmetric with respect to the middle of the tunnel during the whole simulation. Figure 16 clearly indicates that the tunnel slope leads to a significant flow velocity in the direction of the tunnel exit, which restricts an increasing temperature at the lower part of the tunnel.

5. CONCLUSION

In the present paper, we studied a new fluid dynamics model which is used to model low-Mach number flows in combination with large energy transport. The model was applied to simulate fire events in vehicle tunnels, where standard models from computational fluid dynamics seem to fail. The system is discretized using a modification of a standard projection method based on finite-differences and numerical results were given for two realistic fire events. The model should be seen as a physically motivated alternative to compressible flow models on one hand and incompressible equations on the other hand. Both types of models are known to run into difficulties when modelling low-Mach number flows in combination with strong heat transfer.

Concerning fire events in vehicle tunnels we concentrate on the most important effects occurring in the flow. The model has to be generalized to the case of large tunnel slopes, ventilation systems in the tunnel, to the case of air supply systems, etc. Moreover, one may
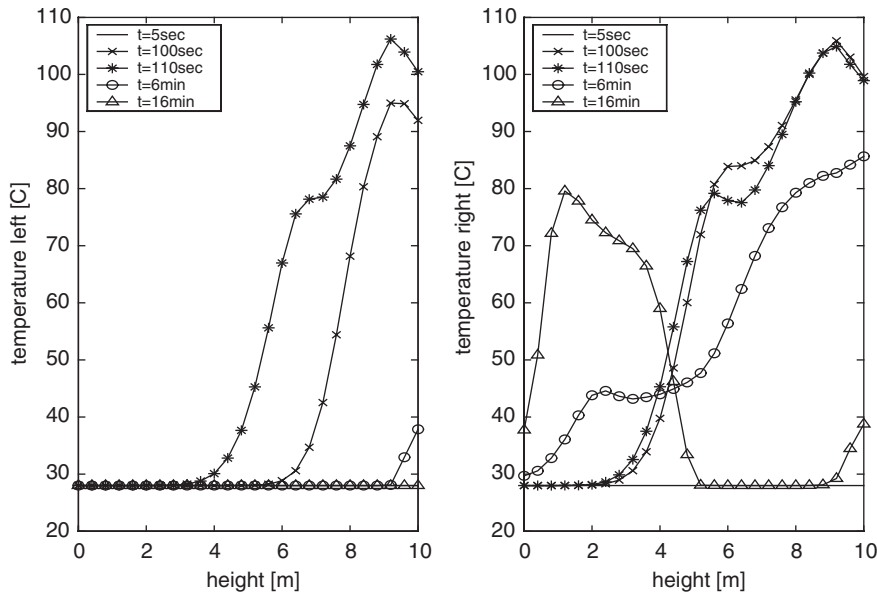
Figure 16. Vertical temperature profiles (in °C) for a tunnel with slope 100 m left and right from the heat source at various times.

take into account radiative heat transfer. A further generalization concerns the modelling of turbulence. Some work in these directions is presently under investigation.

REFERENCES

1. Grant GB, Jagger SF, Lea CJ. Fires in tunnels. *Philosophical Transactions of the Royal Society of London Series A* 1998; **356**:2873–2906.
2. PIARC 1999 Fire and smoke control in road tunnels, *PIARC Commettre on Road Tunnels* (*C5*), 05.05.B, World Road Association, 1999.
3. Lions PL. *Mathematical Topics in Fluid Dynamics. Volume I*: *Incompressible Models*. Clarendon Press; Oxford, 1996.
4. Gray DD, Giorgini A. The validity of the Boussinesq approximation for liquids and gases. *International Journal of Heat and Mass Transfer* 1976; **19**:545–551.
5. Lions PL. *Mathematical Topics in Fluid Dynamics. Volume II*: *Compressible Models*. Clarendon Press; Oxford, 1998.
6. Gasser I, Struckmeier J. An asymptotic induced one-dimensional model to describe fires in tunnels. *Mathematical Modelling in Applied Sciences* 2002; **25**:1231–1249.
7. Almgren AS, Bell JB, Colella P, Howell LH, Welcome ML. A conservative adaptive projection method for the variable density incompressible Navier–Stokes equations. *Journal of Computational Physics* 1998; **142**:1–46.
8. Bell JB, Marcus DL. A second-order projection method for variable-density flows. *Journal of Computational Physics* 1992; **101**:334–348.

9. Welch J, Harlow FH, Shannon JP, Daly BJ. *The MAC Method a Computing Technique for Solving Viscous*, *Incompressible*, *Transient Fluid-Flow Problems Involving Free Surfaces*. Los Alamos Scientific Laboratory California; LA-3425, 1966.
10. Griebel M, Dornseifer T, Neunhoeffer T. *Numerical Simulation in Fluid Dynamics*: *A Practical Introduction*. SIAM; Philadelphia, PA, 1997.
11. Tom M, McKee S. GENSMAC: A computational marker and cell method for free surface flows in general domains. *Journal of Computational Physics* 1994; **110**:171–186.